2024 European Control Conference (ECC)
June 25-28, 2024. Stockholm, Sweden

Data-Driven Observer Design for Nonlinear Vehicle Dynamics using Deep Radial Basis Function Networks with Delay Compensation

Hasan Abdl Ghani, Xincheng Zhuang, Sofiane Ahmed Ali, Haoping Wang, Redouane Khemmar

Abstract— **This study presents a novel approach for estimating lateral velocity, an important parameter for vehicle stability characterization. Aiming to resolve the problems of poor estimation accuracy caused by the insufficient modeling of traditional model-based methods and issues with sampled and delayed measurements, a sampled delay data neural network method for lateral velocity estimation is designed. Our approach incorporates a compensating injector to fill information gaps between samples, an extended compensation dynamic to reduce delays' impact, and a radial basis function neural network to mimic vehicle motions. Continuous weight updates ensure adaptability, and stability is demonstrated using the Lyapunov methodology. Experimental results confirm the effectiveness of our approach, providing promising insights to enhance lateral velocity estimation and improve control and stability in autonomous vehicle systems.**

I. INTRODUCTION

The incidence of traffic accidents has increased as car ownership has become more widespread [1]. Active Control Systems (ACSs), including Traction Control Systems (TCSs), Electronic Stability Program (ESP), and Active Front Wheel Steering (AFS), are now standard in vehicles to enhance safety and reduce accidents. Advanced driver assistance systems (ADAS), like Adaptive Cruise Control (ACC) and Lane Keeping Assistance (LKA), are also gaining popularity. However, challenges such as expensive sensors, complex measurement noise, and restricted sensor accuracy may hinder the accurate measurement of fundamental vehicle states, such as lateral velocity, yaw rate, and sideslip angle. Overcoming these challenges is crucial for ACSs and ADAS to operate effectively and improve vehicle safety.

Lateral velocity plays a crucial role in a vehicle's dynamic and kinematic response [2]. It significantly influences stability evaluation and efficient control implementation by providing essential insights into the vehicle's sideways motion. Accurate prediction of lateral velocity is vital for optimizing vehicle control systems, facilitating precise trajectory tracking, and promoting stability control. Thus, acquiring accurate and reliable lateral velocity data is imperative for enhancing vehicle security and overall performance.

Automobile engineering is actively focused on estimating lateral velocity or sideslip angle using affordable sensors and estimation methods. This study can be categorized into neural network (NN)-based methods and model-based methods. Model-based approaches utilize kinematic and dynamic models to establish relationships between the sideslip angle and other vehicle parameters [3,4]. While effective, these methods face challenges due to the nonlinearity of vehicle models and varying operational conditions. In contrast, neural network models offer advantages by describing vehicle dynamics without explicit knowledge of underlying parameters [5]. By employing appropriate model structures and diverse training data, neural network-based methods have shown promising results in accurately estimating the vehicle's dynamic state. Early neural network observers, primarily designed for Single Input Single Output (SISO) systems, laid the foundation [6]. While initially based on the strict positive real (SPR) basis, later studies expanded to more general nonlinear systems with multiple inputs and outputs (MIMO). For instance, a two-layer Neural Network Observer (NNO) architecture without the SPR assumption was developed using improved back-propagation (BP) algorithms [7]. Chen *et al.* [8] investigated uncertainty's impact on lithium-ion battery system output and introduced an RBF neural network (RBFNN)-based adaptive observer. Moreover, NN observers were applied to estimate vehicle roll angles through sensor fusion with a linear Kalman filter [9].

Despite the success of previous observers across various domains, a notable limitation is their assumption of continuous variables. In reality, data from accessible sensors is inherently discrete, sampled at specific intervals. When these observers are deployed on digital signal processors, the sampling rate of sensors becomes critical, affecting observer convergence. Bridging the gap between discrete system output and continuous state estimation is challenging. The field of sampled data nonlinear neural observers (SDNNO) remains largely unexplored, despite advances in sampled data observer literature ([10],[11]). Hasan *et al.* proposed incorporating an output predictor into the neural network observer framework to achieve continuous estimation of discrete data [12]. Meanwhile, Hu *et al.* created a deterministic learning high-gain observer under sampling conditions, though it was based in discrete system modeling and incapable of achieving continuous state estimation [18].

The problem of time delays is often overlooked compared to sampling measurements, yet it poses significant challenges. Information flow between system components and information processing capacity naturally lead to delays in processes and systems. Ignoring delays can result in instability and poor system performance. Time-varying delay systems have been studied previously for comparison [13,14].

Building upon the preceding discussion, this paper pro-

This work is co-founded by the ANR (French National Agency) through the ARTISMO project and supported by IUT of Évry Val d'Essonne.

poses a new sampled data neural network observer to enhance the accuracy of vehicle lateral velocity estimation amidst signal sampling delay and modeling uncertainty.

The remainder of this paper is organized as follows: Section 2 offers an introduction to the dynamic model of automatic ground vehicles, accompanied by a thorough problem description. Section 3 presents the design and stability analysis of the novel neural network adaptive observer, which has been specifically designed to address the challenges posed by sampled-delayed output. In Section 4, we demonstrate the practical validation of our proposed method by implementing it on an autonomous ground vehicle and showcasing the experimental results.

II. PROBLEM STATEMENT

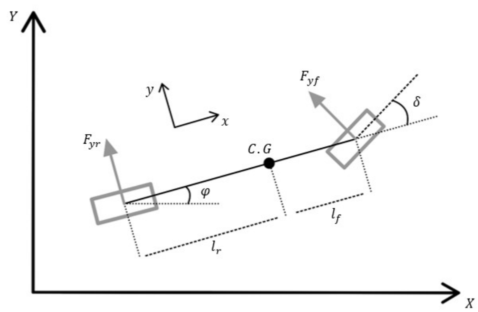

Fig. 1. 2-DOF bicycle model of the vehicle

A. DYNAMIC BICYCLE MODEL

A vehicle prototype with a two-degree-of-freedom configuration is shown Fig.1. This specific model has been used frequently in numerous research projects to examine the lateral dynamic properties of vehicles. It develops by using Newton's second law to assess the vehicle's lateral and longitudinal movements [15]:

$$\begin{cases} \dot{v}_x = -\frac{F_{yf}\sin\delta + F_a}{m} \\ \dot{v}_y = \frac{F_{yf}\cos\delta + F_{yr}}{m} - rv_x \\ \dot{r} = \frac{F_{yf}l_f\cos\delta - F_{yr}l_r}{I_z} \end{cases} \tag{1}$$

In the context of the vehicle's perspective, we use the terms "longitudinal velocity" to refer to the velocity in the direction of motion (v_x), "lateral velocity" to represent the velocity perpendicular to the direction of motion (v_y), and "rotational velocity" to indicate the speed of rotation (r). The lateral forces acting on the front and rear tires are respectively denoted as F_{yf} and F_{yr}. The force responsible for acceleration generated by the vehicle's motors or deceleration produced by the brakes is symbolized as F_a. This force can be computed using the equation $F_a = ma_x$, where a_x represents the inertial acceleration of the vehicle at its center of gravity in the x-axis direction. The control input, which refers to the steering angle of the front tire, is represented as δ. Experimental evidence [16] suggests that for small slip angles, the relationship between the lateral force and the slip angle can be approximated linearly. Taking this into account, the front and rear tire forces are modeled using a linear tire force model, which can be expressed as:

TABLE I
PARAMETER VALUES OF VEHICLE MODEL

Parameter	Description	Value
m	Vehicle Mass	600 [kg]
I_z	Vehicle yaw moment of inertia	1100 [kgm^2]
l_f	Distance from CoG to front axle	0.86 [m]
l_r	Distance from CoG to rear axle	0.9 [m]
C_f	Front cornering stiffness	27500 [N/rad]
C_r	Rear cornering stiffness	27500 [N/rad]

$$F_{yf} = 2C_f\alpha_f + f_{yf}(\alpha_f); F_{yr} = 2C_r\alpha_r + f_{yr}(\alpha_r) \tag{2}$$

In the given tire force model, C_f and C_r are the linear coefficients associated with the front and rear tire forces, while α_f and α_r represent the slip angles of the front and rear wheels, respectively. When the slip angles are small, we can approximate α_f and α_r using the following expressions:

$$\alpha_f = \delta - \frac{v_y}{v_x} - \frac{l_f r}{v_x}; \alpha_r = -\frac{v_y}{v_x} + \frac{l_r r}{v_x} \tag{3}$$

Assuming that the steering wheel angles are small, we can approximate $\sin(\delta)$ as δ. By applying this approximation, Equation (1) can be rewritten in state space form. In this form, the states are represented by v_x, v_y, and r, while the control inputs consist of the steering angle δ and the longitudinal acceleration a_x.

$$\begin{aligned} \dot{x} &= A(u(t), y(t))x + g(u(t), x(t)) \\ y &= Cx \end{aligned} \tag{4}$$

In the given context, the state vector is denoted as $x \in \mathbb{R}^3$, representing a vector in n-dimensional real space. The output matrix is represented as $y \in \mathbb{R}^2$, indicating a vector in p-dimensional real space. The term $A(u, y) \in \mathbb{R}^{3\times3}$ corresponds to the nonlinear components, which can vary with the control input u and the output y. The term $g(u, x) \in \mathbb{R}^3$ represents an unknown nonlinear term, which can also depend on the control input u and the state vector x.

$$\begin{gathered} A = \begin{bmatrix} 0 & 0 & \frac{2C_f l_f \delta}{mv_x} \\ 0 & -\frac{2C_f + 2C_r}{mv_x} & 0 \\ 0 & \frac{2l_rC_r - 2l_fC_f}{Izv_x} & 0 \end{bmatrix}, C = \begin{bmatrix} 1 \ 0 \ 0 \\ 0 \ 0 \ 1 \end{bmatrix}, \\ g = \begin{bmatrix} \frac{2C_f\delta}{mv_x}v_y + a_x \\ (-v_x + \frac{2l_rC_r - 2l_fC_f}{mv_x})r + \frac{2C_f}{m}\delta \\ -\frac{2l_f^2C_f + 2l_r^2C_r}{I_zv_x}r + \frac{2C_fl_f}{I_z}\delta \end{bmatrix}. \end{gathered} \tag{5}$$

B. Problem Statement and Preliminaries

The objective of this paper is to estimate the lateral velocity, represented as v_y, of a vehicle in situations where the vehicle dynamics given by equation (4) are not known. Furthermore, it is assumed that the measurements of the longitudinal speed, denoted as v_x, and the yaw rate, denoted as r, are affected by periodic sampling and a certain amount of delay. This problem can be formulated using the following state equation:

$$\begin{cases} \dot{x}(t) & = Ax + g(u(t), x(t)) \\ y(t_k) & = Cx(t_k) \\ y_\Delta(t) & = y(t - \Delta(t)) \end{cases} \tag{6}$$

were $\Delta \in \mathbb{R}$ is a periodic delay with an upper bound Δ_M. In this research, the unknown dynamics $g(u(t), x(t))$ are estimated using RBFNN (Radial Basis Function Neural Network). Before discussing the approximation concept of RBFNN, certain assumptions are made to establish the requirements for the network. These assumptions define the constraints and criteria that need to be satisfied in order to effectively utilize RBFNN for the estimation task.

Assumption 1: The unknown nonlinear term $g(u(t), z(t))$ is defined in compacts sets.

According to the mentioned assumption, $g(u(t), z(t))$ can be approximated by RBFNN as follows:

$$g(u(t), x(t)) = \Phi(\omega)\xi + \epsilon \tag{7}$$

In the given context, the input of the neural network is denoted as $\omega = [u, x]^T$, where u represents the control input and x represents the state vector. The weight of the neural network is represented by $\xi \in \mathbb{R}^m$, which captures the parameters to be learned by the network. The activation functions used in the network are included in the matrix $\Phi(\omega) \in \mathbb{R}^{3\times m}$, where n represents the dimension of the state vector and m represents the number of activation functions. The approximation error is denoted as $\epsilon \in \mathbb{R}^3$, indicating the difference between the estimated dynamics and the true dynamics.

Each element, denoted as $\Phi_{i,j}(\omega)$, within the matrix $\Phi(\omega)$ represents a Gaussian function characterized as follows:

$$\Phi_{i,j}(\omega) = \exp\left(-\frac{||\omega - c_j||^2}{b_j^2}\right), \tag{8}$$

In the Gaussian function, c_j represents the center and b_j denotes the width of the function. The radial basis function neural network $\Phi(\omega)\xi$ can approximate the unknown element $g(u(t), x(t))$ effectively with a negligible error ϵ if the weight ξ is chosen appropriately. The subsequent analysis is based on the following crucial assumption:

Assumption 2: The weight vector ξ is defined within a compact set, bounded by $\xi_M > 0$. The approximation error ϵ is bounded by an upper bound $\epsilon_M > 0$

This assumption, which is commonly used in neural network approximation [10], plays a fundamental role in the analysis. It is important to note that the Lipschitz and bounded properties of Φ can be easily verified.

III. Observer Design and Stability Analysis

In this section, we introduce a novel approach called the Sampled-delay-Data Neural Network Observer (SDDNNO), which is specifically designed to estimate and observe the behavior of the unknown system described by equation (7):

$$\dot{\hat{x}} = A\hat{x} + \Phi(u, \hat{x})\hat{\xi} - (S^{-1}C^T + \beta P\Omega^T)\eta \tag{9}$$

$$\begin{cases} \dot{\eta}_\Delta = -C(S^{-1}C^T + \beta P\Omega^T)\eta(t - \Delta(t)) + K_2\eta_\Delta(t) \\ \quad \text{for } t \in [t_i, t_{k+1}) \\ \dot{S}(t) = -\theta_s S(t) - A(u, \hat{y})^T S(t) - S(t)A(u, \hat{y}) + C^T C \\ \eta_\Delta(t_i) = \hat{y}(t_i - \Delta(t_i)) - y(t_i - \Delta(t_i)) \end{cases} \tag{10}$$

with

$$\eta = \eta_\Delta + \int_{t-\Delta(t)}^{t} [-C(S^{-1}C^T + \beta P\Omega^T)\eta(s) + K_3\eta(s)]ds \tag{11}$$

In the proposed approach, we denote the state estimation as $\hat{x} \in \mathbb{R}^3$, the compensated output error as $\eta \in \mathbb{R}^2$, and the weight estimation as $\hat{\xi} \in \mathbb{R}^m$. We define $\hat{y} = C\hat{x}$, where C is a given matrix, $\Omega = C\beta$, and $P \in \mathbb{R}^{m\times m}$ is a symmetric positive definite (SPD) matrix that needs to be designed. Additionally, $K_2 \in \mathbb{R}^{2\times 2}$ and $K_3 \in \mathbb{R}^{2\times 2}$ are design parameters, and $\eta_\Delta \in \mathbb{R}^3$ represents the compensation for delayed output error. Moreover, $\beta \in \mathbb{R}^{3\times m}$ is an auxiliary variable defined as follows:

$$\dot{\beta} = (A - S^{-1}C^T C)\beta + \Phi(u, \hat{x}) \tag{12}$$

Assumption 3: For $t \leq 0$, we define $\lambda_m(S)$ and $\lambda_M(S)$ such that the solution of $S(t)$ for the Riccati equation in (11) satisfies the following conditions:

$$\lambda_m(S)I \leq S(t) \leq \lambda_M(S)I \tag{13}$$

It is crucial to note that the matrix $A(u, y)$ is time-varying, which means that designing an observer with a gain L that satisfies $(A(u, \hat{y}) - LC)$ has the potential to destabilize the system.

Remark 1: If it is assumed that $(A(u, \hat{y}) - S^{-1}C^T C)$ is stable, where $S(t)$ is the solution of the Riccati equation in (12), and Φ is bounded, then it can be inferred that β is also bounded.

The observer structure comprises three parts. The first part, as shown in equation (10), is responsible for estimating the state of the system (7). The second part, represented by equation (11), specifically provides compensation for the delayed output error. On the other hand, equation (12) provides compensation for the non-delayed output error. We can now proceed with the central contribution of the paper:

Theorem 1: Under Assumption 1-3, system (10-12) is a SDDNNO for system (7). Moreover, the neural network weight update law is designed as:

$$\dot{\hat{\xi}} = -P\Omega^T\eta - \kappa\xi \tag{14}$$

where $\kappa > 0$ is a design parameter. If the sampling interval upper bound denoted by τ_M and delay upper bound Δ_M satisfy:

$$\begin{cases} 0 < ||K_3||\sigma_1(\Delta_M) < 1 \\ 0 < \vartheta_1(\Delta_M, \tau_M) < 1 \end{cases} \tag{15}$$

then the estimation error of both state and weight are uniformly ultimately bounded (UUB). We define:
$\rho_0=\kappa-\dfrac{\alpha}{2}-\dfrac{\gamma}{4}$,
$\ni$ constant ρ such that $0<\rho<\rho_0/2$,
$\vartheta_1\left(\Delta_M, \tau_M\right)=\dfrac{2 \gamma_5 c_1\left(\sigma_1\left(\tau_M\right)+\sigma_2\left(\Delta_M\right)\right)}{\rho_0\left(1-\left\|K_3\right\| \sigma_2\left(\Delta_M\right)\right)}$,
$\vartheta_2\left(\Delta_M, \tau_M, \epsilon\right)=\dfrac{2 \gamma_5 \epsilon_1 \sigma_2\left(\Delta_M\right)}{\rho_0\left(1-\left\|K_3\right\| \sigma_2\left(\Delta_M\right)\right)}+\dfrac{2 \gamma_3}{\rho_0}$,
$\sigma_1\left(\tau_M\right)=\displaystyle\int_0^{\tau_M} e^{(\|K_2\|+\rho) s} d s, \sigma_2\left(\Delta_M\right)=\dfrac{e^{\rho \Delta_M}-1}{\rho}$,
$\gamma=\gamma_1+\gamma_2, \alpha=2 \rho_a L_{\Phi} \xi_M, \gamma_1=2 \rho_b L_{\Phi} \xi_M \beta_M$
$\gamma_2=2 \rho_b \beta_M, \Phi_M=\sup\limits_{t \geq 0}||\Phi(t)||$,
$\gamma_5=max\left(||K_2||\sqrt{\underline{\lambda}(S)}, \Omega_M\sqrt{\bar{\lambda}(P)}\right)$
$\rho_a=\sqrt{\bar{\lambda}(S)/\underline{\lambda}(S)}, \sigma_1(\tau_M)=\displaystyle\int_0^{\tau_M} e^{(||K_2||+\rho)} s d s$,
$c_1=max\Big((\mu+||C||L_{\Phi}\xi_M)/\sqrt{\underline{\lambda}(S)}$,
$((\mu+||C||L_{\Phi}\xi_M)\beta_M+||C||\Phi_M)\sqrt{\lambda_M(P)}\Big)$,
$\mu=||CA-K_2C||, \beta_M=\sup\limits_{t\geq 0}||\beta||, \Omega_M=\sup\limits_{t\geq 0}||\Omega||$,
$\rho_b=\sqrt{\bar{\lambda}(S)\bar{\lambda}(P)}, c_2=c_0+\dfrac{2\omega_5}{\rho_0}\epsilon_1\sigma_1\left(\tau_M\right)$
$\gamma_5=\dfrac{2 c_5}{\rho_0} c_1 \sigma_1\left(\tau_M\right), \gamma_6=\dfrac{2 \gamma_3}{\rho_0}, c_0=e^{\rho_0 t_0} V_s\left(t_0\right)$,
$\epsilon_1=\|C \epsilon\|, \gamma_3=\sqrt{\lambda_M(S)}\left(\epsilon_M+\beta_M \xi_M\right)+\dfrac{\xi_M^2}{2 \lambda_m(P)}$
$V_s\left(t_0\right)=\sqrt{\zeta^T(0) S \zeta(0)}+\sqrt{\tilde{\xi}^T(0) P^{-1} \tilde{\xi}(0)}$.
Proof. Establish the state and weight errors as $\tilde{x}=\hat{x}-x$ and $\tilde{\xi}=\hat{\xi}-\xi$, it derives:

$$\begin{cases}\dot{\tilde{x}}=A_k\tilde{x}+\tilde{\Phi}(\delta,\hat{x},x)\xi+\Phi(\delta,\hat{x})\tilde{\xi}-\epsilon+\beta\dot{\tilde{\xi}}\\ \qquad+\kappa\beta\tilde{\xi}-\kappa\beta\xi+S^{-1}C^Te_w\\ \dot{\tilde{\xi}}=-P\Omega^TC\tilde{x}-\kappa\tilde{\xi}+\kappa\xi+P\Omega^Te_w\end{cases} \tag{16}$$

with $A_k=A-S^{-1}C^TC$,$e_w=\tilde{\omega}-\eta, \tilde{\Phi}(\delta,\hat{x},x)=\Phi(\delta,\hat{x})-\Phi(\delta,x)$. Perform the designated coordinate transformation as indicated in [17], which is:

$$\zeta(t)=\tilde{x}(t)-\beta(t)\tilde{\xi}(t) \tag{17}$$

Differentiating $\zeta(t)$ w.r.t. time, one has:

$$\dot{\zeta}=A_k\zeta-\epsilon+\tilde{\Phi}(\delta,\hat{x},x)\xi+\kappa\beta\tilde{\xi}-\kappa\beta\xi+S^{-1}C^Te_w \tag{18}$$

Consider the following Lyapunov function candidate:

$$V(\zeta,\tilde{\xi})=V_\zeta(\zeta)+V_\xi(\tilde{\xi}) \tag{19}$$

with

$$V_\zeta(\zeta)=\zeta^TS\zeta \tag{20}$$

$$V_\xi(\tilde{\xi})=\tilde{\xi}^TP^{-1}\tilde{\xi} \tag{21}$$

where S is the solution of Riccati equation in (11). The proof will be segmented into three parts. In the first part, we will concentrate on illustrating the Input-to-State Stability (ISS) characteristic of e_w concerning V_s. The second part will affirm the ISS property of V_s concerning e_w. Lastly, the third part will utilize the small gain method to conclude the proof.Due to space limitations, only a sketch of the proof will be provided. Let's commence by demonstrating the ISS characteristic from e_w to V_s. To initiate, we differentiate $V_\zeta(\zeta)$ with respect to time:

$$\begin{aligned}\dot{V}_\zeta(\zeta)=&-\theta_sV_\zeta(\zeta)+2\zeta^TSA_k\zeta+2\zeta^TS\tilde{\Phi}(\delta,\hat{x},x)\xi\\&-2\zeta^TS\epsilon+2\kappa\zeta^TS\beta\tilde{\xi}-2\kappa\zeta^TS\beta\xi+2\zeta^TCe_w\end{aligned} \tag{22}$$

Taking into account equation (18), we derive:

$$\|\tilde{x}\|\leqslant\|\zeta\|+\|\beta\|\|\tilde{\xi}\|\leqslant\|\zeta\|+\beta_M\|\tilde{\xi}\| \tag{23}$$

By implementing the subsequent scaling to the components within equation (23), we acquire:

$$\begin{aligned}&2\zeta^TS\tilde{\Phi}(\delta,\hat{x},x)\xi\leqslant2\sqrt{\bar{\lambda}(S)}\sqrt{V_\zeta(\zeta)}L_\Phi\xi_M\|\tilde{x}\|\\&\leqslant\alpha V_\zeta+\omega_1\sqrt{V_\zeta}\sqrt{V_\xi}\\&2\kappa\zeta^TS\beta\tilde{\xi}\leqslant2\sqrt{\bar{\lambda}(S)}\sqrt{V_\zeta(\zeta)}\beta_M\|\tilde{\xi}\|\\&\leqslant\omega_2\sqrt{V_\zeta}\sqrt{V_\xi}\end{aligned} \tag{24}$$

with

$$\begin{aligned}&\omega=\omega_1+\omega_2,\alpha=2\rho_aL_\Phi\xi_M,\omega_1=2\rho_bL_\Phi\xi_M\beta_M,\\&\omega_2=2\rho_b\beta_M,\rho_a=\sqrt{\bar{\lambda}(S)/\underline{\lambda}(S)},\rho_b=\sqrt{\bar{\lambda}(S)\bar{\lambda}(S)}.\end{aligned} \tag{25}$$

By merging equation (23) with equation (25), we deduce:

$$\begin{aligned}\dot{V}_\zeta(\zeta)\leqslant&-\zeta^TS\zeta-\zeta^TC^TC\zeta+(\alpha-\theta_s)V_\zeta+\omega\sqrt{V_\zeta}\sqrt{V_\xi}\\&+2\sqrt{\lambda_M(S)V_\zeta}\epsilon_M+2\sqrt{\lambda_M(S)V_\zeta}\beta_M\xi_M\\&+2\left\|K_1\right\|\sqrt{\bar{\lambda}(S)V_\zeta}\|e_w\|\end{aligned} \tag{26}$$

Conversely, let's differentiate $V_\xi(\zeta)$ concerning time:

$$\begin{aligned}\dot{V}_\xi(\tilde{\xi})=&-2\kappa V_\xi-\tilde{\xi}^T\Omega^T\Omega\tilde{\xi}-2\tilde{\xi}^T\Omega^TC\zeta\\&+2\tilde{\xi}^T\Omega^Te_w+2\kappa\tilde{\xi}^TS^{-1}\xi\\\leqslant&-\kappa V_\xi-\tilde{\xi}^T\Omega^T\Omega\tilde{\xi}-2\tilde{\xi}^T\Omega^TC\zeta\\&+2\Omega_M\sqrt{V_\xi\bar{\lambda}(S)}\|e_w\|+\xi_M^2/\lambda_m(S)\end{aligned} \tag{27}$$

Let us denote $V_s=\sqrt{V_\zeta}+\sqrt{V_\xi}$, combining equations (27) and (28), we obtain:

$$\dot{V}_s\leqslant-\rho_0V_s+\omega_4\|e_w\|+\omega_3 \tag{28}$$

with $\omega_3=\sqrt{\lambda_M(S)}\left(\epsilon_M+\beta_M\xi_M\right)+\frac{\xi_M^2}{2\lambda_m(S)}$, $\omega_4=\max\left(\left\|K_1\right\|\sqrt{\underline{\lambda}(S)},\Omega_M\sqrt{\bar{\lambda}(P)}\right)$. By integrating both sides of equation (29) with respect to time, and then multiplying both sides by $e^{\rho t}$ and assuming $0<\rho<\rho_0/2$, we obtain:

$$e^{\rho t}V_s\leqslant c_0+\frac{2\omega_3}{\rho_0}e^{\rho t}+\frac{2\omega_4}{\rho_0}\sup_{t_0\leqslant s\leqslant t}\left(e^{\rho s}\|e_w\|\right) \tag{29}$$

We can deduce that the connection between e_w and V_s demonstrates Input-to-State Stability (ISS). To establish ISS from V_s to e_w, let's proceed with the proof. Suppose $e_w = \tilde{\omega} - \eta$, then we derive:

$$\begin{aligned}\|e_w\| \leqslant & \|e_{w\Delta}\| + c_1 \frac{e^{-\rho t}\left(e^{\rho\Delta_M}-1\right)}{\rho} \sup_{t-\Delta_M \leqslant s \leqslant t}\left(e^{\rho s} V_s\right) \\ & + \|K_3\| \frac{e^{-\rho t}\left(e^{\rho\Delta_M}-1\right)}{\rho} \sup_{t-\Delta_M \leqslant s \leqslant t}\left(e^{\rho s}\|e_w(s)\|\right) \\ & + \epsilon_1 \frac{e^{-\rho t}\left(e^{\rho\Delta_M}-1\right)}{\rho \leqslant s \leqslant t}\left(e^{\rho s}\right)\end{aligned} \tag{30}$$

By multiplying both sides of equation (35) by $e^{\rho t}$, and taking $\sigma_2\left(\Delta_M\right) = \frac{e^{\rho\Delta_M}-1}{\rho}$, and then selecting Δ_M such that

$$0 < \|K_3\| \sigma_2\left(\Delta_M\right) < 1 \tag{31}$$

We have:

$$\begin{aligned}\sup_{t_0 \leqslant s \leqslant t}\left(e^{\rho s}\|e_w\|\right) \leqslant & \left(\sup_{t_0 \leqslant s \leqslant t}\left(e^{\rho s}\left\|e_{w\Delta}\right\|\right)\right. \\ & + c_1\sigma_2\left(\Delta_M\right) \sup_{t_0 \leqslant s \leqslant t}\left(e^{\rho s} V_s\right) \\ & \left. + \epsilon_1\sigma_2\left(\Delta_M\right) \sup_{t_0 \leqslant s \leqslant t}\left(e^{\rho s}\right)\right) / \left(1 - \|K_3\| \sigma_2\left(\Delta_M\right)\right)\end{aligned} \tag{32}$$

Also:

$$\begin{aligned}e^{\rho t}\left\|e_{w\Delta}\right\| \leqslant & c_1\sigma_1\left(\tau_M\right) \sup_{t_i \leqslant s \leqslant t}\left(e^{\rho s} V_s(s-\Delta(s))\right) \\ & + \epsilon_1\sigma_1\left(\tau_M\right)\end{aligned} \tag{33}$$

Combing (38) and (39), one has:

$$\begin{aligned}& \sup_{t_0 \leqslant s \leqslant t}\left(e^{\rho s}\|e_w\|\right) \leqslant \\ & \frac{\underset{t_0 \leqslant s \leqslant t}{c_1\sigma_1\left(\tau_M\right) \sup\left(e^{\rho s} V_s(s-\Delta(s))\right) + \epsilon_1\sigma_1\left(\tau_M\right)}}{1 - \|K_3\| \sigma_2\left(\Delta_M\right)} + \\ & \frac{c_1\sigma_2\left(\Delta_M\right) \sup_{t_0 \leqslant s \leqslant t}\left(e^{\rho s} V_s\right) + \epsilon_1\sigma_2\left(\Delta_M\right) \sup_{t_0 \leqslant s \leqslant t}\left(e^{\rho s}\right)}{1 - \|K_3\| \sigma_2\left(\Delta_M\right)}\end{aligned} \tag{34}$$

We will now conclude the proof using the small gain method. By merging (42) and (33), we have:

$$\begin{aligned}e^{\rho t} V_s(t) \leqslant & c_0 + \frac{2\gamma_3}{\rho_0} e^{\rho t} + \frac{2\gamma_4}{\rho_0} \sup_{t_0 \leqslant s \leqslant t}\left(e^{\rho s}\|e_w\|\right) \\ \leqslant & c_3 + \vartheta_1\left(\Delta_M, \tau_M\right) \sup_{0 \leqslant s \leqslant t}\left(e^{\rho s} V_s\right) \\ & + \vartheta_2\left(\Delta_M, \tau_M, \epsilon\right) e^{\rho t}\end{aligned} \tag{35}$$

Let Δ_M and τ_M satisfy

$$\vartheta_1\left(\Delta_M, \tau_M\right) < 1 \tag{36}$$

Combined with (42), one gets:

$$\sup_{t_0 \leqslant s \leqslant t} e^{\rho s} V_s(s) \leqslant \frac{c_3 + \vartheta_2\left(\Delta_M, \tau_M, \epsilon\right) e^{\rho t}}{1 - \vartheta_1\left(\Delta_M, \tau_M\right)} \tag{37}$$

Following (42), one has:

$$V_s(t) \leqslant \frac{c_3 e^{-\rho t} + \vartheta_2\left(\Delta_M, \tau_M, \epsilon\right)}{1 - \vartheta_1\left(\Delta_M, \tau_M\right)} \tag{38}$$

Following (45) and using $V_s = \sqrt{V_\zeta} + \sqrt{V_\xi}$

$$\begin{cases}\|\zeta\| \leqslant \dfrac{c_3 e^{-\rho t} + \vartheta_2\left(\Delta_M, \tau_M, \epsilon\right)}{\sqrt{\lambda(S)}\left(1 - \vartheta_1\left(\Delta_M, \tau_M\right)\right)} \\ \|\xi\| \leqslant \dfrac{\sqrt{\bar{\lambda}(P)}\left(c_3 e^{-\rho t} + \vartheta_2\left(\Delta_M, \tau_M, \epsilon\right)\right)}{1 - \vartheta_1\left(\Delta_M, \tau_M\right)}\end{cases} \tag{39}$$

combined with (24), it can be derived that:

$$\begin{aligned}\|\tilde{x}\| \leqslant & \frac{c_3 e^{-\rho t} + \vartheta_2\left(\Delta_M, \tau_M, \epsilon\right)}{\sqrt{\underline{\lambda}(S)}\left(1 - \vartheta_1\left(\Delta_M, \tau_M\right)\right)} \\ & + \frac{\theta_M \sqrt{\bar{\lambda}(P)}\left(c_3 e^{-\rho t} + \vartheta_2\left(\Delta_M, \tau_M, \epsilon\right)\right)}{1 - \vartheta_1\left(\Delta_M, \tau_M\right)}\end{aligned} \tag{40}$$

Thus $\tilde{x}$ and $\tilde{\xi}$ are UUB. The proof ends.

IV. EXPERIMENTAL RESULTS

In this section, we validate our proposed observer through experiments conducted with the Citroen AMI experimental vehicle, shown in Fig.4, at the IRSEEM facility in Rouen, France. We present the results alongside a comparative analysis with the Kalman filter, as detailed in [21], highlighting our observer's superior performance in real-world scenarios. The experimental procedure began with the vehicle starting at a speed of 30.6 km/h (8.5 m/s) as it navigated through a road crossing and completed half of a roundabout circuit twice. This scenario is depicted in Fig.2, which also illustrates the precise steering input required to accurately follow the intended path. Detailed specifications and attributes of the vehicle used in the experiment are listed in Table 1. Furthermore, Fig.3 addresses the variable delay considered during the experiment.

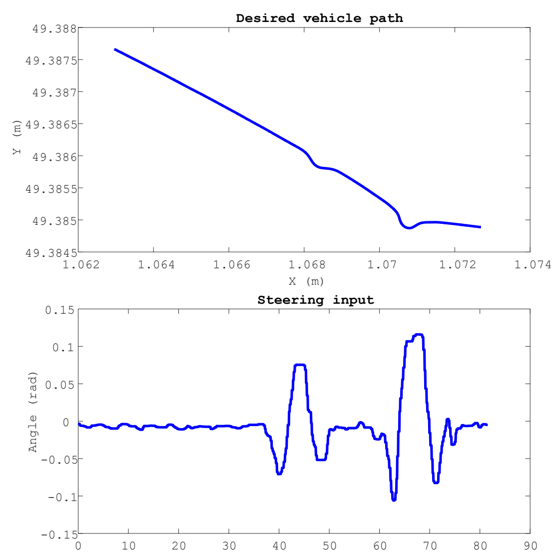

Fig. 2. RTMaps experimental results: Desired vehicle path and steering input.

Fig. 4. Experimental vehicle Citröen AMI

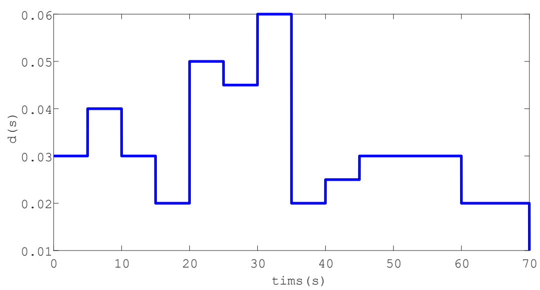

Fig. 3. Evolution of the random delay d(t)

A random sample time T_s was selected within the range 0.05 to 0.15. The experiment utilized a hidden layer of 15 neurons and parameters $\beta(0) = 0_{3\times15}$, $K_2 = 20I_2$, $K_3 = 30I_2$, $P = 20\text{diag}(0.1I_{15}, 7I_{15}, I_{15})$, and $\kappa = 0.4$. Comparative analysis with a Kalman filter designed for delay compensation in vehicle state estimation showed that our observer outperforms in handling delays, as shown in Fig.5. It demonstrated greater adaptability to varying delays, providing more accurate and responsive state estimates. This underscores the observer's effectiveness and reliability for real-time vehicle state estimation, especially where precise delay compensation is crucial, surpassing the traditional Kalman filter.

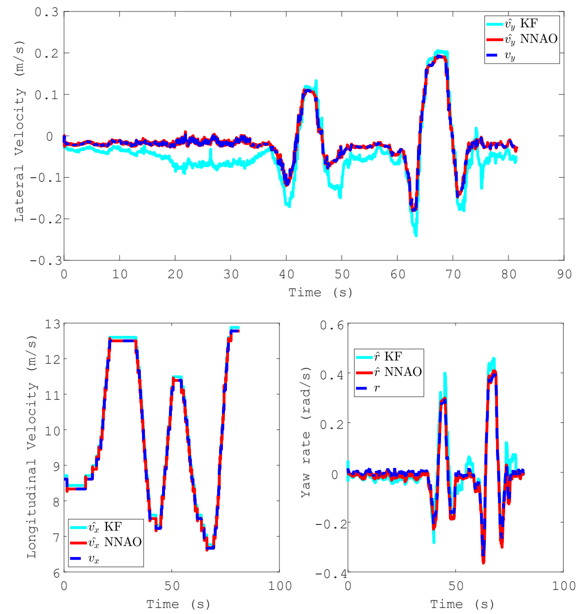

Fig. 5. RTMaps experimental results : estimation of vehicle state variables.

References

[1] D. Piyabongkarn, R. Rajamani, J. A. Grogg and J. Y. Lew, "Development and experimental evaluation of a slip angle estimator for vehicle stability control," American Control Conference, pp. 6, 2006.

[2] H. A. Ghani, H. Laghmara, S. A. Ali and S. Ainouz, "Neural Network Observer for Lateral Vehicle Model with Varying Sampled and Delayed Output," 2023 62nd IEEE Conference on Decision and Control (CDC), Singapore, Singapore, 2023, pp. 5358-5363.

[3] M. Doumiati, A. C. Victorino, A. Charara and D. Lechner, "Onboard Real-Time Estimation of Vehicle Lateral Tire–Road Forces and Sideslip Angle," in IEEE/ASME Transactions on Mechatronics, vol. 16, no. 4, pp. 601-614, Aug. 2011.

[4] M.C. Best, T.J. Gordon and P.J. Dixon, "An Extended Adaptive Kalman Filter for Real-time State Estimation of Vehicle Handling Dynamics," in Vehicle System Dynamics, vol. 34, no. 1, pp. 57-75, 2000.

[5] A. N. Lakhal, A. S. Tlili, N. B. Braiek, "Neural Network Observer for Nonlinear Systems Application to Induction Motors 1," International Journal of Control and Automation, 2010.

[6] D. Strobl, U. Lenz and D. Schroder, "Systematic design of stable neural observers for a class of nonlinear systems," Proceedings of the 1997 IEEE International Conference on Control Applications, Hartford, CT, USA, pp. 377-382, 1997.

[7] F. Abdollahi, H. A. Talebi and R. V. Patel, "A stable neural network-based observer with application to flexible-joint manipulators," IEEE Transactions on Neural Networks, vol. 17, no. 1, pp. 118-129, Jan. 2006.

[8] N. Chen, X. Zhao, J. Chen, X. Xu, P. Zhang, W. Gui," Design of a Non-Linear Observer for SOC of Lithium-Ion Battery Based on Neural Network," Energies 2022, 15, 3835.

[9] L. V. Meléndez, , B. L. Boada, M.-J. L. Boada, AA. Gauchía and V. Díaz, "A Sensor Fusion Method Based on an Integrated Neural Network and Kalman Filter for Vehicle Roll Angle Estimation," vol. 16, no. 9, 2016.

[10] I. Karafyllis and C. Kravaris, "From Continuous-Time Design to Sampled-Data Design of Observers," in IEEE Transactions on Automatic Control, vol. 54, no. 9, pp. 2169-2174, Sept. 2009.

[11] I Karafyllis, T. Ahmed-Ali, F. Giri, "A note on sampled-data observers," Systems & Control Letters, vol. 144, 2020.

[12] A.-G. Hasan, H. Laghmara, A.-A. Sofiane, S. Ainouz, G. Xing, "Continuous–Discrete Time Neural Network Observer for Nonlinear Dynamic Systems Application to Vehicle Systems," in 22nd World Congress of the International Federation of Automatic Control, Jul 2023.

[13] Q.-T. Dam, R.- H. Thabet, A.-A. Sofiane, F.G, A.-G. Hasan, "A High-Gain Observer Design for Nonlinear System with Delayed Measurements: Application to a Quadrotor UAV," in 22nd World Congress of the International Federation of Automatic Control, Jul 2023.

[14] M.-A. Pakzad, "Kalman Filter Design for Time Delay Systems," WSEAS Transactions on Systems, no. 11, pp. 551-560, 2012.

[15] R. Rajamani, Vehicle Dynamics and Control. Springer US, 2012.

[16] H. Pacejka, Tire and vehicle dynamics. Elsevier 2005.

[17] Q. Zhang, "Adaptive observer for multiple-input-multiple-output (MIMO) linear time-varying systems," in IEEE Transactions on Automatic Control, vol. 47, no. 3, pp. 525-529, March 2002.

[18] J. Hu, W. Wu, B. Ji and C. Wang, "Observer Design for Sampled-Data Systems via Deterministic Learning," in IEEE Transactions on Neural Networks and Learning Systems, vol. 33, no. 7, pp. 2931-2939, July 2022.